

# Quantum photocell based on GaN quantum dots

Abhishek Chakraborty\* and Vishvendra Singh Poonia†

Indian Institute of Technology, Roorkee

(Dated: December 29, 2020)

In this work, we propose an efficient photocell based on GaN quantum dots. We exploit the strong built-in electric field in GaN QDs and excitonic dipole-dipole coupling between adjacent QDs to break detailed balance. This is a much stronger effect than Fano interference, and we show that such a photocell exhibits enhanced photo-voltage and photocurrent over its conventional counterpart. The proposed quantum photocell could be the first step towards harnessing quantum effects in practical energy harvesting devices.

## I. INTRODUCTION

Photovoltaic or solar cells are one of the most promising options for clean energy. A major challenge in the design of solar cells is their low efficiency. It was shown by Shockley and Queisser[1] that the limited efficiency is due to electron-hole pairs lost due to radiative recombination before charge separation can occur to extract useful work from them, a consequence of detailed balance. Quantum dot solar cells (QDSCs) have been proposed as an alternative to p-i-n solar cells to overcome some of the other drawbacks of conventional photocell design. Tandem cells with different bandgaps would utilise a larger part of the solar spectrum, increasing the overall efficiency of a solar panel. Other approaches extract energy from hot charge carriers [2]. We propose an alternative biologically inspired photocell design, which uses quantum interference to achieve enhanced efficiency. In our proposed design, excitonic dipole-dipole coupling in GaN quantum dots creates a dark state, which reduces radiative recombination by breaking detailed balance, resulting in increased efficiency. In section II, we introduce the two-level system model for QDs used to design the photocell, then describe the model with and without coupling. In section III, we calculate the tunneling rates for charge carriers in and out of the dots. This is used to perform numerical simulations, the results of which are presented in section IV.

## II. TWO-LEVEL SYSTEM MODEL

The design we want to analyze is simply that of a p-i-n photocell with the intrinsic semiconductor region replaced by a two-level quantum dot. (as shown in Figure 1)

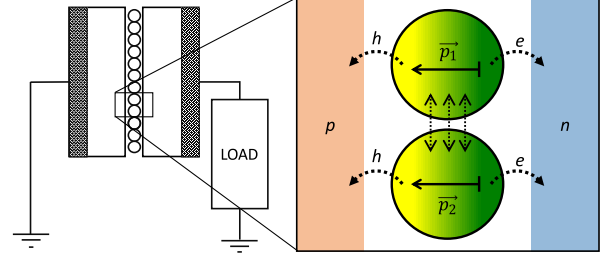


FIG. 1. Schematic of QDSC with GaN QDs and dipole-dipole coupling

### A. Excitonic dipole-dipole coupling

In a realistic model, we can consider two identical adjacent quantum dots such that the total two-dot system can be thought of as having two degenerate excited states. For the uncoupled dots, we label the ground state (no exciton in QD) as  $|g\rangle$  and first excited state (one exciton in QD) as  $|e\rangle$ . Since these are excitonic states, i.e. bound states of electrons and holes, they have a nonzero dipole moment. If the two quantum dots are close enough, the exciton in one dot will experience the electric field due to the excitonic dipole moment from the other dot and vice-versa. This dipole-dipole interaction will lead to a modification of the excitonic energy spectrum for the two-dot system. If we consider the two excitonic dipoles at position vectors  $\vec{r}_1$  and  $\vec{r}_2$  with electric dipole moments  $\vec{\mu}_1$  and  $\vec{\mu}_2$  respectively. The electric fields generated at position vector  $\vec{r}$  by these dipoles are  $\vec{E}_1(\vec{r})$  and  $\vec{E}_2(\vec{r})$  respectively. The change in energy of a dipole due to the electric field generated by the other dipole is given by

$$\Delta\mathcal{E} = -\vec{\mu}_2 \cdot \vec{E}_1(\vec{r}_{21}) = -\vec{\mu}_1 \cdot \vec{E}_2(\vec{r}_{12}) \quad (1)$$

where  $\vec{r}_{21} = -\vec{r}_{12} = \vec{r}_2 - \vec{r}_1 \equiv d_\perp$  equal to the perpendicular QD spacing. In our case, we assume that both the dipole moments are parallel and equal in magnitude ( $\vec{\mu}_1 = \vec{\mu}_2 = \vec{\mu}$ ). The electric field due to a dipole at a point on the perpendicular bisector plane is

$$\vec{E}_{dip}^\perp(\vec{r}) = -\frac{1}{4\pi\epsilon} \frac{\vec{\mu}}{r^3} \quad (2)$$

\* Department of Computer Science and Engineering

† Department of Electronics and Communication Engineering; vishvendra@ece.iitr.ac.in

With this, the energy shift becomes

$$\Delta\mathcal{E} = \frac{|\vec{\mu}|^2}{4\pi\epsilon d_{\perp}^3} \equiv J \quad (3)$$

where  $J$  denotes the coupling strength between the two dipoles. We can construct a configuration such that the interaction is perfectly *coherent* and thus no energy leaks out from the system into the radiation field. This is done by ensuring that the interdot spacing  $d_{\perp} \ll 1/k$  where  $k$  is the wavevector associated with the transition in the dots. To find the new excitonic spectrum, we must diagonalize the total Hamiltonian for the two-dot system with the dipole-dipole interaction included.

$$H = H_0 + H_1 \quad (4)$$

$$H_0 = \sum_{j=1,2} \hbar\omega_j \sigma_j^+ \sigma_j^- \text{ and } H_1 = J(\sigma_1^+ \sigma_2^- + \text{h.c.}) \quad (5)$$

The uncoupled Hamiltonian  $H_0$  is already diagonal and we can represent its eigenstates in terms of the single QD eigenstates. The total system ground state  $|b\rangle$  is one where both QDs are in their respective ground states i.e.  $|g_1g_2\rangle$ . There is one doubly degenerate (in the energy eigenvalue) excited state corresponding to only one of the two QDs being in the excited state  $|e\rangle$  while the other is in state  $|g\rangle$ . We label these eigenstates as  $|a_1\rangle \equiv |e_1g_2\rangle$  and  $|a_2\rangle \equiv |e_2g_1\rangle$  both corresponding to the energy eigenstate  $\mathcal{E}_{ab}$ . Finally the second excited state of the system corresponds to both QDs being in the excited state  $|e\rangle$ . This state is  $|e_1e_2\rangle \equiv |a^*\rangle$  with energy eigenvalue  $2\mathcal{E}_{ab}$ . The effect of the interaction Hamiltonian  $H_1$  is to allow mixing of these states, and hence, the energy spectrum also changes. It is clear from (5) that the interaction only facilitates transitions between states  $|a_1\rangle$  and  $|a_2\rangle$  and hence the lowermost and uppermost states will remain unchanged.

Upon diagonalizing the total Hamiltonian, we obtain the new excitonic energy spectrum. This is shown in Figure 2.

The coupled system has modified eigenstates  $|b\rangle, |x_1\rangle, |x_2\rangle$  and  $|a^*\rangle$  where

$$\begin{aligned} |x_1\rangle &= \frac{1}{\sqrt{2}}(|a_1\rangle + |a_2\rangle) \\ |x_2\rangle &= \frac{1}{\sqrt{2}}(|a_1\rangle - |a_2\rangle) \end{aligned} \quad (6)$$

The energy eigenvalues of these new eigenstates are given by

$$\mathcal{E}_{x_{1,2}} = \mathcal{E}_{ab} \pm J \quad (7)$$

Now, we will analyze the allowed transitions between these levels under illumination. Ideally, we would like to analyze the effects of solar radiation, but since we are dealing with only a few levels, we will only be concerned with radiation of a particular frequency tuned to the energy gap between the desired levels in our two-dot

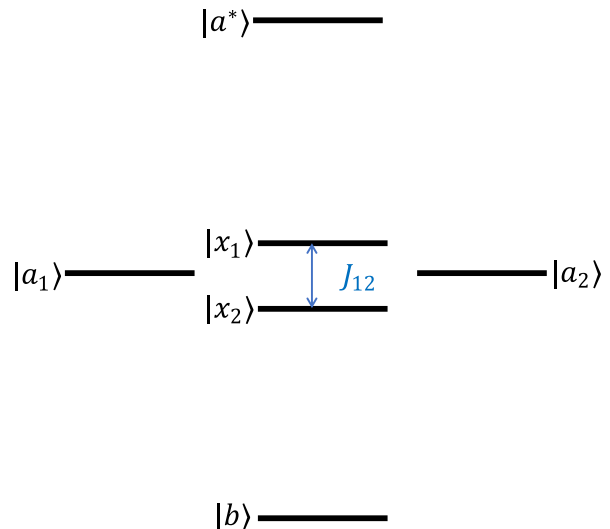


FIG. 2. The energy diagram of the two TLS quantum dots with and without dipole-dipole coupling.

system. For our photocell, we will not use the  $|a^*\rangle$  level. Since the state  $|b\rangle$  has no dipole moment either, we will only be concerned with the dipole moments of the intermediate states. We will further concern ourselves with a pumping field that is parallel to the dipole moment of the exciton. Practically, this can be realized using a polarizing filter. From the Weisskopf-Wigner theory of spontaneous decay, we know that the transition rate between two levels is given by

$$\gamma = \frac{\omega^3 |\mu|^2}{\hbar\pi\epsilon_0 c^3} \propto |\mu|^2 \quad (8)$$

Here,  $\hbar\omega$  is the energy of the photon field tuned to the energy gap between the concerned levels and  $|\mu|$  is the magnitude of the transition dipole moment. Now, given that the dipole moment (absolute value) for both the states  $|a_{1,2}\rangle$  is equal to  $|\mu|$ , we can find the corresponding value for the new eigenstates  $|x_{1,2}\rangle$  as below

$$|\mu_{1,2}| = \frac{1}{\sqrt{2}} |\mu_1 \pm \mu_2| \quad (9)$$

Thus, we see that for the symmetric eigenstate  $|x_1\rangle$ , the transition dipole moment is  $\sqrt{2}$  times larger than the uncoupled eigenstates, while for the antisymmetric eigenstate it is zero. We define the transition rate between the ground state and the symmetric eigenstate as

$$\gamma_h = \frac{2\omega_{1b}^3 |\mu|^2}{\hbar\pi\epsilon_0 c^3} \quad (10)$$

where  $\hbar\omega_{1b} = \mathcal{E}_{x_1}$  is the energy associated with the pumping transition. We note that the transition rate between the ground state and the symmetric eigenstate is twice that of the uncoupled eigenstates, while transitions between the ground state and antisymmetric eigenstate are

forbidden, making this state a *dark state*. Since this dark state has no dipole moment, all radiative transitions involving this state are forbidden. Therefore, other pathways must be used to populate and depopulate this state. We will consider transitions mediated by electron-phonon interactions as the major cause of the decay of  $|x_1\rangle$  to  $|x_2\rangle$ . LO-phonon-electron interactions lead to ultrafast decays [3] in III-V semiconductors and hence it is reasonable to assume this is much faster than the radiative recombination between  $|x_1\rangle$  and the ground state  $|b\rangle$ . Since the  $|x_2\rangle$  state is dark, there cannot be a radiative relaxation to the ground state. We further argue that, due to the large energy difference, a phonon-mediated relaxation to the ground state is much less likely than tunnelling of the electron out of the dot (provided there is an available energy level outside the dot). In our case, this effect is augmented, in part, by the built-in electric field in GaN quantum dots. We will examine this shortly.

### B. Charge separation and work extraction for the photocell

In order to create a charge-separated state to extract work from our photocell, we need two more levels aside from the QD energy spectrum. We will call these levels  $|\alpha\rangle$  and  $|\beta\rangle$ . The electron from the exciton tunnels through the QD barrier into state  $|\alpha\rangle$  where the QD is now left with a net positive charge. The electron now passes through some form of an electrical load, and the system relaxes to another state  $|\beta\rangle$  following which an electron from the bulk semiconductor tunnels into the QD and recombines with the hole to return the whole system to the ground state  $|b\rangle$ . The complete energy level scheme for this process for systems with and without coupling are shown in Figure 5 and Figure 4 respectively.

The two levels  $|\alpha\rangle$  and  $|\beta\rangle$  are still improperly defined in terms of their energy values. So we will discuss the physical origins of the transitions involving these states and justify their energy structure. It is clear from the band diagram in Figure 3 that the conduction band minimum (CBM) on the n-doped side is below the excitonic state energy level. This is by design and tunnelling is allowed from the excitonic levels to the conduction band, since we assume that there are available energy levels above the conduction band minimum. Once the electron has tunnelled out of the quantum dot, it becomes a *hot* electron in the bulk semiconductor, i.e. a carrier with energy higher than the CBM. This hot-electron now relaxes to the CBM via the same ultrafast LO-phonon mediated transition as we considered earlier and is discussed in [3]. Since this transition is much faster than the tunnelling rate, as we will show later, we consider the tunnelling process to be the rate-limiting step in this entire process and consider the relaxation to the CBM to be nearly instantaneous. Similar arguments apply to the tunnelling of the hole out of the dot to the valence band on the p-doped side. Hence, for convenience, we will consider  $|\alpha\rangle$

to be the CBM on the n-doped bulk semiconductor surrounding the dot and  $|\beta\rangle$  to the valence band maximum (VBM) on the p-doped bulk semiconductor.

Now, we will put forth the reasons we have chosen GaN QDs as the material of choice for our coherence-enhanced photocell. Firstly, GaN-based quantum dots with a wurtzite crystal structure in AlGaIn bulk semiconductor, there is a strong built-in electric field [4]. This field has contributions both a spontaneous polarization charge induced at the GaN/AlGaIn interface, and a strain-induced piezoelectric field at the GaN/AlGaIn interface [5], and the latter dominates in the case of GaN quantum dots due to the lack of an inversion centre in the Wurtzite crystal structure. Due to the differing cell dimensions for GaN and AlGaIn from the usual hexagonal structure, the spontaneous polarization is also an appreciable effect and is around the same order of magnitude and in the same direction as the piezoelectric field [6]. It is also noted that the magnitude of the electric field is roughly equal both inside and immediately outside the dots, although there is a change in direction. The resul-

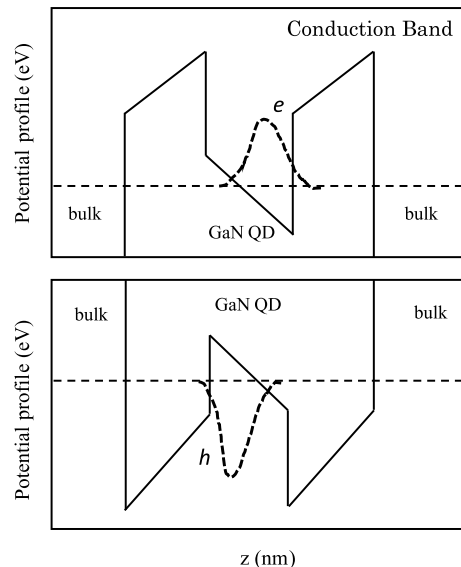


FIG. 3. Potential profile for the GaN QD in the presence of the built-in electric field.

tant potential profile for the GaN quantum dot can be seen in Figure 3. This improves the lateral confinement of the exciton. The dipole moment of the exciton aligns with the intrinsic electric field, and here we will assume that the separation of charges is equal to the longitudinal dimension of the quantum dot. This is reasonable given the structure of the potential in Figure 3. However, due to this separation of charges, there is a monotonic decrease in the excitonic binding energy as compared to a flat band [5] which will aid the tunnelling of electrons in and out of the quantum dots.

Based on the above description, we will now derive the Pauli master equations for both coupled and uncoupled photocells and measure the current enhancement.

### C. Uncoupled Model

The energy level scheme for the uncoupled system of two GaN quantum dots with their dipoles aligned is shown in Figure 4. Both the quantum dots experience

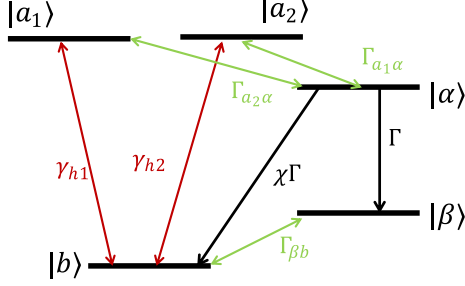


FIG. 4. Energy level scheme for photocell with uncoupled QDs

a similar environment in the growth direction, but the interdot spacing is too large to allow dipole-dipole coupling. The interaction Hamiltonian in the interaction picture for the two-QD system interacting with an incoherent photonic field is

$$\mathcal{V}(t) = \hbar \sum_{\mathbf{k}} g_{\mathbf{k}} \hat{a}_{\mathbf{k}} e^{i(\omega - \nu_{\mathbf{k}})t} \hat{S}_1^\dagger + \hbar \sum_{\mathbf{q}} g_{\mathbf{q}} \hat{a}_{\mathbf{q}} e^{i(\omega - \nu_{\mathbf{q}})t} \hat{S}_2^\dagger + \text{h.c.} \quad (11)$$

where  $\hat{a}_{\mathbf{k}}$  ( $\hat{a}_{\mathbf{k}}^\dagger$ ) is the annihilation (creation) operator for a photon with energy  $\hbar\nu_{\mathbf{k}}$ . Note here that  $\nu_{\mathbf{k}}$  is used here to denote angular frequency.  $\hat{S}_i^\dagger$  ( $\hat{S}_i$ ) is the raising (lowering) operator for the  $i^{\text{th}}$  QD.  $g_{\mathbf{k}}$  denotes the coupling constant of the transition to the photon mode of energy  $\hbar\nu_{\mathbf{k}}$ . Since there is no effective interaction between the dots, we neglect the exchange of virtual photons between the two dots. To obtain the dynamics of this system, we substitute the interaction picture interaction Hamiltonian (11) into the Liouville-von Neumann equation of motion with a manually inserted dissipation term [7]

$$\dot{\rho} = \frac{-i}{\hbar} [\mathcal{V}(t), \rho] - \frac{1}{2} \{\Gamma, \rho\} \quad (12)$$

The density operator in the above equation is also taken in the interaction picture. Next, we trace over the photonic reservoir using techniques discussed earlier, and we get the equation of motion for the reduced density matrix for the photocell

$$\begin{aligned} \frac{d\rho}{dt} = & -\frac{\gamma_{1h}}{2} \left[ (\bar{n}_{1h} + 1) (\hat{S}_1^\dagger \hat{S}_1 \rho - 2\hat{S}_1 \rho \hat{S}_1^\dagger + \rho \hat{S}_1^\dagger \hat{S}_1) \right. \\ & \left. + \bar{n}_{1h} (\hat{S}_1 \hat{S}_1^\dagger \rho - 2\hat{S}_1^\dagger \rho \hat{S}_1 + \rho \hat{S}_1 \hat{S}_1^\dagger) \right] \\ & -\frac{\gamma_{2h}}{2} \left[ (\bar{n}_{2h} + 1) (\hat{S}_2^\dagger \hat{S}_2 \rho - 2\hat{S}_2 \rho \hat{S}_2^\dagger + \rho \hat{S}_2^\dagger \hat{S}_2) \right. \\ & \left. + \bar{n}_{2h} (\hat{S}_2 \hat{S}_2^\dagger \rho - 2\hat{S}_2^\dagger \rho \hat{S}_2 + \rho \hat{S}_2 \hat{S}_2^\dagger) \right] \end{aligned} \quad (13)$$

Taking matrix elements of the density operator in the basis vectors for the states we described in the previous section and defining  $\rho_{ij} \equiv \langle i | \rho | j \rangle$  we get the following Pauli master equations.

$$\begin{aligned} \dot{\rho}_{a_1 a_1} &= -\gamma_{1h} [(1 + n_{1h}) \rho_{a_1 a_1} - n_{1h} \rho_{bb}] - \Gamma_{a_1 \alpha} \rho_{a_1 a_1} \\ \dot{\rho}_{a_2 a_2} &= -\gamma_{2h} [(1 + n_{2h}) \rho_{a_2 a_2} - n_{2h} \rho_{bb}] - \Gamma_{a_2 \alpha} \rho_{a_2 a_2} \\ \dot{\rho}_{\alpha \alpha} &= \Gamma_{a_1 \alpha} \rho_{a_1 a_1} + \Gamma_{a_2 \alpha} \rho_{a_2 a_2} - (\Gamma + \chi \Gamma) \rho_{\alpha \alpha} \\ \dot{\rho}_{\beta \beta} &= \Gamma \rho_{\alpha \alpha} - \Gamma_{\beta b} \rho_{\beta \beta} \\ \rho_{a_1 a_1} + \rho_{a_2 a_2} + \rho_{\alpha \alpha} + \rho_{\beta \beta} + \rho_{bb} &= 1 \end{aligned} \quad (14)$$

In the equations above, we have also included a spontaneous decay term  $\Gamma$ , where the anticommutator simplifies to a single term in case of Pauli master equations. We manually insert the decay factors in the equations based on the level scheme. Here,  $n_{ih}$  is the number of ambient solar photons tuned to the exciton excitation energy.  $\Gamma_{a_i \alpha}$  is the electron tunneling rate which takes the photocell system from the state  $|a_i\rangle$  to  $|\alpha\rangle$  and  $\Gamma_{\beta b}$  is the hole tunneling rate which takes the system from state  $|\beta\rangle$  to  $|b\rangle$ . Since both states  $|a_i\rangle$  are identical and in identical environments, we will consider them equal. Similarly, since the energy levels  $|a_i\rangle$  are degenerate, their spontaneous decay rates will be equal and so will the number of ambient solar photons.

$$\begin{aligned} \Gamma_{a_1 \alpha} &= \Gamma_{a_2 \alpha} \equiv \Gamma_{\alpha \alpha} \\ \gamma_{1h} &= \gamma_{2h} \equiv \frac{\gamma_h}{2} \\ n_{1h} &= n_{2h} \equiv n_h \end{aligned} \quad (15)$$

With these simplifications, the Pauli master equations for the uncoupled photocell system are

$$\begin{aligned} \dot{\rho}_{a_1 a_1} &= -\frac{\gamma_h}{2} [(1 + n_h) \rho_{a_1 a_1} - n_h \rho_{bb}] - \Gamma_{\alpha \alpha} \rho_{a_1 a_1} \\ \dot{\rho}_{a_2 a_2} &= -\frac{\gamma_h}{2} [(1 + n_h) \rho_{a_2 a_2} - n_h \rho_{bb}] - \Gamma_{\alpha \alpha} \rho_{a_2 a_2} \\ \dot{\rho}_{\alpha \alpha} &= \Gamma_{\alpha \alpha} \rho_{a_1 a_1} + \Gamma_{\alpha \alpha} \rho_{a_2 a_2} - (\Gamma + \chi \Gamma) \rho_{\alpha \alpha} \\ \dot{\rho}_{\beta \beta} &= \Gamma \rho_{\alpha \alpha} - \Gamma_{\beta b} \rho_{\beta \beta} \\ \rho_{a_1 a_1} + \rho_{a_2 a_2} + \rho_{\alpha \alpha} + \rho_{\beta \beta} + \rho_{bb} &= 1 \end{aligned} \quad (16)$$

We have expressed these equations in terms of  $\gamma_h$  which is the spontaneous decay rate for the coupled case, which is also twice as large as the uncoupled case.

### D. Coupled Model

In the coupled model, we consider the dipole-dipole coupling between nearest neighbour dots only (as can be achieved by tuning the interdot distance), and we use the modified excitonic energy spectrum developed earlier and apply the analysis of the previous section to derive the Pauli Master Equations for this system. The energy level diagram of the system is shown in Figure 5.

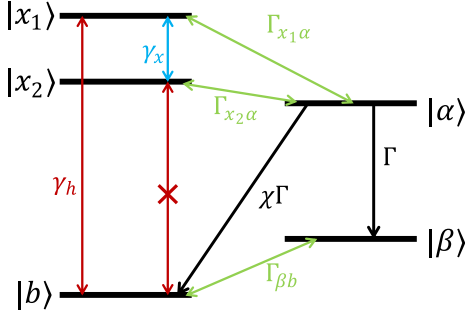


FIG. 5. Energy level scheme for photocell with dipole-dipole coupled QDs

As discussed earlier,  $|x_2\rangle$  is an optically dark state, and hence no optical transitions are allowed for that state. The states  $|b\rangle$  and  $|x_1\rangle$  are coupled by an incoherent photonic field and the states  $|x_1\rangle$  and  $|x_2\rangle$  are coupled by the LO-phonons in GaN. Since investigations into the phonon spectrum of GaN QDs are still in early stages, especially for the kind of configuration we are considering, we will resort to a Planck distribution of LO-phonon modes. This is a good approximation as phononic correlations are significantly negated at room temperature, which is the domain we are interested in, and thus they can be treated as effectively noninteracting bosons. This forms the basis for applying the Markovian approximation on the phononic bath in this case. The dimensions of the GaN QD will be such that the dark state  $|x_2\rangle$  still has an energy greater than the CBM of the surrounding bulk semiconductor to allow tunnelling of electrons and similar considerations will be made for hole tunnelling.

The interaction picture interaction Hamiltonian in this case is

$$\mathcal{V}(t) = \hbar \sum_{\mathbf{k}} g_{\mathbf{k}} \hat{a}_{\mathbf{k}} e^{i(\omega_{1b} - \nu_{\mathbf{k}})t} \hat{\sigma}_{1b}^+ + \hbar \sum_{\mathbf{q}} G_{\mathbf{q}} \hat{b}_{\mathbf{q}} e^{i(\omega_{12} - \nu_{\mathbf{q}})t} \hat{\sigma}_{21}^+ + \text{h.c.} \quad (17)$$

which is similar to (11) except that here  $G_{\mathbf{q}}$  is the exciton-phonon coupling strength,  $\hat{b}_{\mathbf{q}}$  ( $\hat{b}_{\mathbf{q}}^\dagger$ ) is the phonon annihilation (creation) operator and  $\hat{\sigma}_{ij}^+ \equiv |i\rangle\langle j|$  ( $\hat{\sigma}_{ij}^- \equiv |j\rangle\langle i|$ ) is the raising (lowering) operator between  $|j\rangle$  and  $|i\rangle$ . For readability, we have abbreviated  $x_1$  and  $x_2$  to 1 and 2 respectively in these subscripts. Following the same procedure to get the equation of motion for the reduced density operator of the system, we obtain

$$\begin{aligned} \frac{d\rho}{dt} = & \frac{-\gamma_h}{2} [(\bar{n}_h + 1)(\hat{\sigma}_{1b}^+ \hat{\sigma}_{1b}^- \rho - 2\hat{\sigma}_{1b}^- \rho \hat{\sigma}_{1b}^+ + \rho \hat{\sigma}_{1b}^+ \hat{\sigma}_{1b}^-) \\ & + \bar{n}_h(\hat{\sigma}_{1b}^- \hat{\sigma}_{1b}^+ \rho - 2\hat{\sigma}_{1b}^+ \rho \hat{\sigma}_{1b}^- + \rho \hat{\sigma}_{1b}^- \hat{\sigma}_{1b}^+)] \\ & - \frac{\gamma_x}{2} [(\bar{n}_x + 1)(\hat{\sigma}_{21}^+ \hat{\sigma}_{21}^- \rho - 2\hat{\sigma}_{21}^- \rho \hat{\sigma}_{21}^+ + \rho \hat{\sigma}_{21}^+ \hat{\sigma}_{21}^-) \\ & + \bar{n}_x(\hat{\sigma}_{21}^- \hat{\sigma}_{21}^+ \rho - 2\hat{\sigma}_{21}^+ \rho \hat{\sigma}_{21}^- + \rho \hat{\sigma}_{21}^- \hat{\sigma}_{21}^+)] \end{aligned} \quad (18)$$

where  $\gamma_x$  is the spontaneous decay rate from  $|x_1\rangle$  to  $|x_2\rangle$  via LO-phonon mediated relaxation and  $\bar{n}_x$  is the aver-

age thermal occupation of ambient phonons at temperature  $T_a$ , all given by the Planck distribution.

$$\bar{n} = \frac{1}{e^{\Delta\mathcal{E}/(k_B T_a)} - 1} \quad (19)$$

We will again find the specific equations for the diagonal elements for the density operator with the additional decay term to obtain the Pauli Master Equations.

$$\begin{aligned} \dot{\rho}_{x_1 x_1} = & -\gamma_x [(1 + n_x) \rho_{x_1 x_1} - n_x \rho_{x_2 x_2}] \\ & - \gamma_h [(1 + n_h) \rho_{x_1 x_1} - n_h \rho_{bb}] - \Gamma_{x_1 \alpha} \rho_{x_1 x_1} \\ \dot{\rho}_{x_2 x_2} = & \gamma_x [(1 + n_x) \rho_{x_1 x_1} - n_x \rho_{x_2 x_2}] - \Gamma_{x_2 \alpha} \rho_{x_2 x_2} \\ \dot{\rho}_{\alpha \alpha} = & \Gamma_{x_1 \alpha} \rho_{x_1 x_1} + \Gamma_{x_2 \alpha} \rho_{x_2 x_2} - (\Gamma + \chi \Gamma) \rho_{\alpha \alpha} \\ \dot{\rho}_{\beta \beta} = & \Gamma \rho_{\alpha \alpha} - \Gamma_{\beta b} \rho_{\beta \beta} \\ \rho_{x_1 x_1} + \rho_{x_2 x_2} + \rho_{\alpha \alpha} + \rho_{\beta \beta} + \rho_{bb} = & 1 \end{aligned} \quad (20)$$

where symbols have the same meaning as in the previous section.

### III. CALCULATION OF TRANSITION RATES

Here we will calculate the various transition rates and other numerical constants we require to carry out computer simulations for our photocell system. We already have an expression for the incoherent pumping rate due to solar radiation from (8).

Of primary importance is the tunneling rate of electrons and holes out of the quantum dot. Electron tunneling followed by rapid phonon-mediated relaxation to the CBM corresponds to the transition from a state inside the QD to the CBM state  $|\alpha\rangle$ . The actual difference between  $|\alpha\rangle$  and  $|\beta\rangle$  is of little consequence because we only care about current and power enhancement, which does not depend on the absolute value of the open-circuit voltage  $V_{OC}$ . As a simple model, we will evaluate the tunneling rate using the WKB approximation in a method similar to the Gamow theory of alpha decay [8]. The exciton can be treated as loosely bound and, in fact, it is known that the binding energy of the exciton is 2-3 times lower in GaN QDs with a built-in electric field as compared to the flat band case [5]. Thus the transmission coefficient  $T$  can be approximated as

$$T \approx \exp\left(-2 \int_a^b \frac{\sqrt{2m^*|V-E|}}{\hbar}\right) \quad (21)$$

where  $m^*$  is the effective mass,  $E$  is the energy of the single particle and  $V$  is the potential it is tunneling through.  $a$  and  $b$  indicate the classical turning points of the potential. Here, we are also making the assumption that the particle has the same energy on both sides of the barrier. This is true for the average energy in this case since the tunneling is augmented by the in-built electric field and

thermal noise in the semiconductor. The tunneling rate is then given by

$$\Gamma_{i\alpha} = \nu_c T_{i\alpha} \quad (22)$$

where  $\nu_c$  is called the assault frequency, defined to be equal to the frequency of a classical oscillator with the particle mass and energy oscillating inside the QD. To calculate this for electrons, we consider the classically allowed region inside the QD. Due to band bending, this region is less than the total width of the QD.

$$\begin{aligned} \nu_c &= \frac{v}{2R} \\ &= \frac{1}{2R} \sqrt{\frac{2(E^* + F_d w_d/2)}{m_e^*}} \\ &= \frac{1}{2\left(\frac{E^*}{F_d} + \frac{w_d}{2}\right)} \sqrt{\frac{2(E^* + F_d w_d/2)}{m_e^*}} \end{aligned} \quad (23)$$

$E^*$  is the energy of the electron measured from the CBM. With this and the form of the potential known from the parameters given in [4, 9], we can evaluate the tunneling rate for an electron with energy  $E^*$

$$\begin{aligned} \Gamma_{i\alpha} &= \frac{1}{2\left(\frac{E^*}{F_d} + \frac{w_d}{2}\right)} \sqrt{\frac{2(E^* + F_d w_d/2)}{m_e^*}} \\ &\times \exp\left(\frac{-4\sqrt{2m_e^*}}{3\hbar F_d} \left[(\Delta E_c - F_d w_d/2 + F_{br} w_{br} - E^*)^{3/2} - (\Delta E_c - F_d w_d/2 - E^*)^{3/2}\right]\right) \end{aligned} \quad (24)$$

This expression is used to calculate tunneling rates out of the dot and for simplicity, we assume the hole tunneling rate is the same as the electron tunneling rate.

#### IV. RESULTS

Here we present results from our numerical simulations. First, we consider the dynamics of both the coupled and uncoupled photocell systems. (16) and (20) might be stiff for some parameter values. We have used the RADAU implicit Runge-Kutta solver to solve these equations numerically. We have made use of the parameters listed in the Table I for the simulations. Any remaining parameters are mentioned alongside the result.

The Pauli master equations (16) and (20) were solved for 200 ns and the populations of the various levels are plotted in Figure 6. In these simulations, we have used  $w_{br} = 0.5$  nm and  $d_{\perp} = 1.5$  nm. We have also made an assumption that the excitonic dipole is 80% the length of the QD.

$$|\mu| = 0.8 \times w_d \quad (25)$$

TABLE I. Values of several parameters used in this work

Quantity	Symbol	Value	Unit
GaN Bandgap	$E_g$	3.51	eV
Conduction band dislocation	$\Delta E_c$	2.0	eV
Valence band dislocation	$\Delta E_v$	0.7	eV
Electron effective mass	$m_e^*$	0.2	$m_e$
Hole effective mass	$m_h^*$	1.0	$m_e$
Relative permittivity	$\epsilon$	9.6	
Quantum dot width	$w_d$	2.7	nm
QD intrinsic electric field	$F_d$	0.54	V nm <sup>-1</sup>
Barrier intrinsic electric field	$F_{br}$	0.57	V nm <sup>-1</sup>
Radiative recombination rate	$\chi$	0.20	
Ambient phonon temperature	$T_a$	300	K
Exciton excitation energy	$E_{1b}$	3.25	eV
Number of solar photons	$n_h$	60000	

We have also chosen the levels  $|\alpha\rangle$  and  $|\beta\rangle$  to be the CBM and VBM for GaN respectively. This gives us  $E_{\alpha\beta} = E_g$ . For the results in Figure 6, we have also assumed  $\gamma_x = 2J$  and  $\Gamma = 0.08$ . Our results differ significantly from those of [10–12]. This is expected because we are considering a completely solid-state implementation of the Quantum Heat Engine model presented there, whereas the authors in those works consider molecular states. The key difference here is that the mechanism for charge separation is different. While they use phonon-mediated electron transfer, our model relies on tunnelling and thus the dynamics are also different. For one, our system does not resemble lasing due to the unidirectional nature of the tunnelling transition. Further, we have considered only effects up to the order of the intrinsic electric field strength. We have ignored the Fano-Agarwal interference terms used in [10, 11] as it is a much weaker effect compared to dipole-dipole coupling.

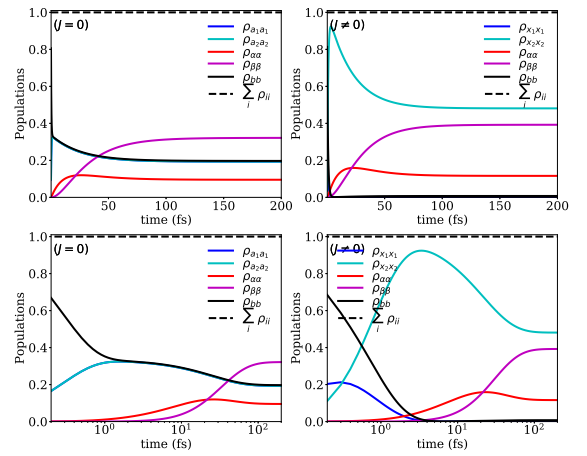


FIG. 6. Population dynamics of both the coupled and uncoupled photocells at 300K. The bottom graphs are in logscale time.

Next, we analyze the I-V and P-V characteristics for both the photocells. For the parameters mentioned above, they are shown in Figure 7. Here we have varied  $\Gamma$ , which has the effect of varying the load on the photocell. To obtain the voltage across the terminals of the photocell, we use

$$eV = E_\alpha - E_\beta + k_b T_a \ln(\rho_{\alpha\alpha}/\rho_{\beta\beta}) \quad (26)$$

The  $\Gamma \rightarrow 0 (j \rightarrow 0)$  corresponds to the open-circuit limit and  $V = 0$  in the short circuit regime. We obtain all quantities from the steady-state solutions of the Pauli master equations. The steady-state current  $j \equiv \Gamma \rho_{\alpha\alpha}$  is shown in the I-V characteristics. For P-V characteristics, we have computed power  $P = j \cdot V$ . As can be seen from the plot, we obtain an enhancement of roughly 25% in this case at peak power. Also, we conclude that this power enhancement occurs in the form of current enhancement because a higher current is drawn in the case of the coupled photocell as compared to the uncoupled one at the same voltage. We have also indicated the power received from the sun  $P_{sun} = j(E_{x_1/a_1} - E_b)/e$  for the coupled and uncoupled case respectively. As we

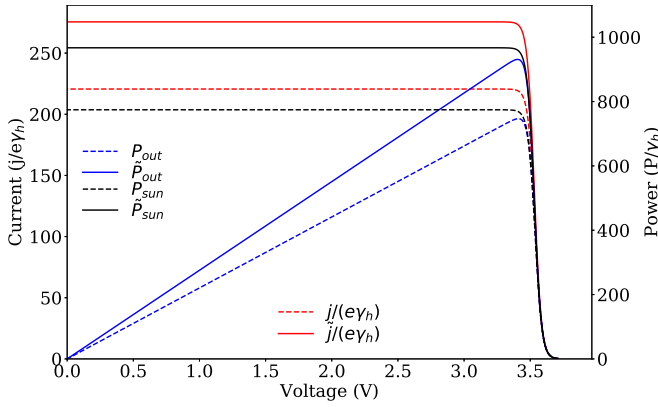


FIG. 7. Current and power enhancement for the coupled and uncoupled photocells. Tildes are used to indicate results from the photocell with dipole-dipole coupling.

can see from the population dynamics, the main factor limiting the efficient operation of our photocell is the slow tunnelling rates. Hence, it is prudent to find an optimal configuration of the photocell geometry in order to extract maximum efficiency from our system. To that end, the parameters that we can control are the interdot spacing  $d_\perp$  and the barrier width  $w_{br}$ . We can evaluate peak relative power efficiency

$$\eta \equiv \frac{\tilde{P}_{out}^{max} - P_{out}^{max}}{P_{out}^{max}} \quad (27)$$

for every configuration. The power efficiency enhancement for the system described here and shown in Figure 7 is 24.6%. Since another unknown factor is the phonon-mediated transition between  $|x_1\rangle$  and  $|x_2\rangle$ , in order to find the regime of maximum efficiency, it is desirable to optimize this parameter too. This is shown

in Figure 8. This is expected behaviour because if the phonon-mediated transition is very weak, the excited level  $|x_1\rangle$  cannot be depleted fast enough to prevent recombination. We also see that the efficiency enhancement starts saturating when the transition rate  $\gamma_x$  is comparable to the dipole-dipole coupling strength  $J$ . Hence, we choose a high value for  $\gamma_x$  to ensure maximum efficiency enhancement. Figure 9 shows the variation of en-

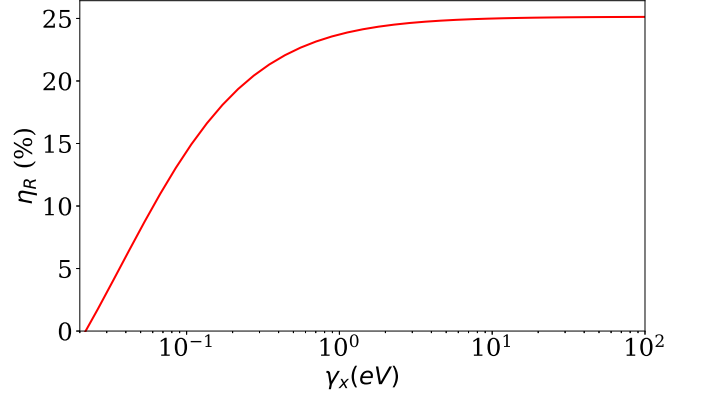


FIG. 8. Relative power enhancement with varying phonon-mediated relaxation to dark state

hanced efficiency with variation in both the perpendicular dot spacing and the barrier width. If the QDs are too far apart, the coupling strength is weak because dipole fields fall off rapidly with distance. On the other hand, if the dots are too close, then lateral confinement will be lost, and tunnelling between the dots will deteriorate the enhancement. Similarly, the barrier width directly affects the transition rates into and out of the quantum dots. However, a balance is struck between these rates and the phonon-mediated relaxation from the symmetric excited state. Thus in the figure, we see a peak representing the ideal balance of these two factors.

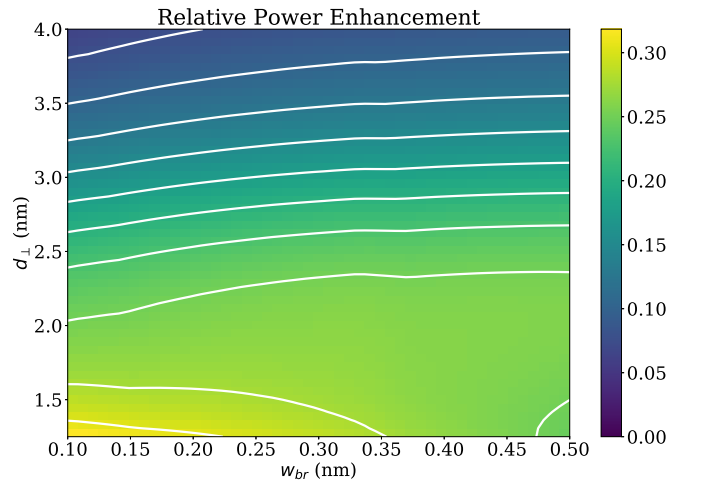


FIG. 9. Relative power enhancement with varying barrier width and interdot spacing

## V. DISCUSSION AND FUTURE WORKS

We have shown that a quantum dot solar cell (QDSC) with dipole-dipole coupling due to the intrinsic electric field in GaN QDs can show a power enhancement of up to 30% over its regular uncoupled counterpart. This makes GaN QDSCs a prime candidate for next-generation solar cells which take advantage of quantum mechanical effects to surpass regular devices operating on principles of classical physics. GaN QDs applications are still in the early stages of research. Further refinements to our model may be possible as more accurate data for GaN QD devices becomes available. One such effect is the so-called *phonon-bottleneck*, which refers to the bandgap in the phonon spectrum of materials. Engineering the phonon bottleneck so that it enhances the phonon-mediated relaxation used in our model can be a source of potential increases in efficiency.

Another aspect we have not explored is the variation of energy level structure of GaN QDs as we change the dimensions of the dot itself. This requires solving a self-consistent Schrodinger equation and Poisson's equation for injected carrier flow rates to obtain the exact energy spectrum of the QDs [3, 4, 6] which is beyond the scope of this work. Engineering the dimensions of the QDs may allow for further enhancements as well. These will be examined in future works. We have also not considered the bulk semiconductor surrounding the QDs. One may look into the best match for such QDSCs so that charge separation is most efficient. This requires studies into the effects of lattice size mismatch and doping on the charge separation efficiency and a more exact derivation of the tunnelling rates based on the exact bandstructure of all semiconductor regions involved, which is also beyond the scope of this work.

- 
- [1] W. Shockley and H. J. Queisser, Detailed balance limit of efficiency of p-n junction solar cells, *Journal of Applied Physics* **32**, 510 (1961).
- [2] A. Nozik, Quantum dot solar cells, *Physica E: Low-dimensional Systems and Nanostructures* **14**, 115 (2002).
- [3] U. Woggon, H. Giessen, F. Gindele, O. Wind, B. Fluegel, and N. Peyghambarian, Ultrafast energy relaxation in quantum dots, *Physical Review B* **54**, 17681 (1996).
- [4] S. D. Rinaldis, I. D'Amico, E. Biolatti, R. Rinaldi, R. Cingolani, and F. Rossi, Intrinsic exciton-exciton coupling in GaN-based quantum dots: Application to solid-state quantum computing, *Physical Review B* **65**, 10.1103/physrevb.65.081309 (2002).
- [5] R. Cingolani, A. Botchkarev, H. Tang, H. Morkoç, G. Traetta, G. Coli, M. Lomascolo, A. D. Carlo, F. D. Sala, and P. Lugli, Spontaneous polarization and piezoelectric field in-gan/al0.15ga0.85nquantum wells: Impact on the optical spectra, *Physical Review B* **61**, 2711 (2000).
- [6] A. D. Andreev and E. P. O'Reilly, Theory of the electronic structure of gan/aln hexagonal quantum dots, *Physical Review B* **62**, 15851 (2000).
- [7] M. Scully and M. Zubairy, *Quantum Optics* (Cambridge University Press, 1997).
- [8] G. Gamow, Zur quantentheorie des atomkernes, *Zeitschrift fur Physik* **51**, 204 (1928).
- [9] S. D. Rinaldis, I. D'Amico, and F. Rossi, Intrinsic electric field effects on few-particle interactions in coupled gan quantum dots, *Physical Review B* **69**, 235316 (2004).
- [10] A. A. Svidzinsky, K. E. Dorfman, and M. O. Scully, Enhancing photovoltaic power by fano-induced coherence, *Physical Review A* **84**, 10.1103/physreva.84.053818 (2011).
- [11] K. E. Dorfman, D. V. Voronine, S. Mukamel, and M. O. Scully, Photosynthetic reaction center as a quantum heat engine, *Proceedings of the National Academy of Sciences* **110**, 2746 (2013).
- [12] C. Creatore, M. A. Parker, S. Emmott, and A. W. Chin, Efficient biologically inspired photocell enhanced by delocalized quantum states, *Physical Review Letters* **111**, 10.1103/physrevlett.111.253601 (2013).